 FDMP, vol.2, no.3, pp.153-165, 2006

Convective Instability in Annular Pools

Y.R. Li[1], L. Peng[1], W.Y. Shi[1] and N. Imaishi[2]

Abstract: The convective instabilities in semiconductor or oxide melts, significantly affect the quality of large crystals grown from the melts by the Czochralski method. This paper reviews our recent numerical studies of thermal convection in annular pools of low-*Pr* silicon melt and moderate-*Pr* silicone oil. The mechanisms of the convective instability are discussed and the critical conditions for the onset of three-dimensional flow are determined. The results show that the hydrothermal wave, characterized by curved spokes, is dominant in a shallow thin pool. In a thick pool of the low-*Pr* silicon melt, there appears a standing wave type of oscillatory longitudinal rolls, which moves in the azimuthal direction and looks very similar to the hydrothermal waves. In deep pools of moderate-*Pr* silicone oil, a three-dimensional steady flow pattern, consisting of pairs of counter-rotating longitudinal rolls, arises, which corresponds to the Rayleigh-Benard instability.

keyword: Convection, Instability, Numerical simulation, Annular pool.

1 Introduction

The Czochralski (Cz) method is one of the most important methods of producing the silicon single crystals from the melt. In this method, heat and mass transfer in the melt are strongly influenced by the melt convection driven by various forces, such as the buoyancy force, the centrifugal and the Coriolis forces due to crystal and crucible rotations, and the thermocapillary force related to the temperature dependence of the surface tension at the melt surface. In the past few decades, thermocapillary flow has been of particular interest in single crystal growth processes of the Cz method, since the melt flow and its spatiotemporal changes cause dopant concentration inhomogeneity in the grown crystals.

Smith and Davis (1983) performed a linear stability analysis of a thin and infinitely extended fluid layer with a free upper surface subjected to a constant horizontal temperature gradient. They found two types of three-dimensional instabilities, i.e. stationary longitudinal rolls and oblique hydrothermal waves (HTWs) depending on the Prandtl number (*Pr*) and the basic flow pattern (with or without a return flow), and determined the critical Marangoni (*Ma*) number. Subsequently, the extension of Smith and Davis' theory to account for the influence of the buoyancy force was done by Laure and Roux (1989) for the low-*Pr* fluids and by Parmentier, Regnier and Lebon (1993) for liquids with *Pr* up to 10. Furthermore, Garnier and Normand (2001) performed a linear stability analysis of radial thermocapillary flow in an extended cylindrical geometry for liquids with *Pr*=10 and predicted that the instability appeared first near the inner cylinder.

After the linear stability analysis of Smith and Davis (1983), many experiments of thermocapillary or thermocapillary–buoyancy convection in liquid layers subjected to a horizontal temperature gradient have been performed for rectangular geometries and annular pools (used as relevant models of the Cz technique). As an example, Riley and Neitzel (1998) and Burguete, Mukolobwiez, Daviaud, Garnier, and Chiffaudel (2001) clearly observed HTWs and obtained a stability limit diagram for the thermocapillary flow in a rectangular channel by plotting the critical temperature difference (ΔT_{cri}) for the incipience of HTWs as a function of the liquid depth. Their results suggest that the critical Marangoni number sensitively increases with the liquid depth. Benz, Hintz, Riley, and Neitzel (1998) demonstrated that HTWs could be suppressed by periodically adding heat onto a liquid surface synchronized with the crests of the hydrothermal waves. Kamotani (1999) conducted a large set of microgravity experiments on oscillatory thermocapillary flow in open cylindrical containers of silicone oil with depths of 12, 20 and 30 mm, in which the liquid was heated from the center. They observed two- or three-lobed surface temperature patterns. Hoyas, Herrero, and Mancho (2002a, 2002b) obtained a stability diagram for these

[1] Chongqing University, Chongqing, China
[2] Kyushu University, Kasuga, Japan

experimental systems by conducting a linear stability analysis. Schwabe, Moller, Schneider, and Scharmann (1992) carried out some experiments on HTWs in shallow annular liquid pools of ethanol (Pr=17) with thickness ranging from 0.6 to 3.6 mm. They observed short-wavelength HTWs with curved (part of spiral) arms in liquid pools with d_o <1.4 mm, and long-wavelength patterns in pools with d>1.4 mm. They also found that gravity significantly stabilizes the basic steady radial thermocapillary flow of silicone oil (Pr=6.8) in an annular silicone oil pool heated from the outer wall, by comparing the results of on-ground experiments and those of a microgravity experiment on the FOTON-12 satellite [Schwabe and Benz (2002), Schwabe, Zebib and Sim (2003)]. Garnier and Chiffaudel (2001) observed HTWs with spiral-like arms in thin annular pools of silicone oil between an inner cold rod with an 8mm diameter and an outer wall with a 135mm diameter, and with a depth of 1.2 or 1.9mm. They observed pulsating, targetlike wave patterns (i.e., coaxial circles traveling outward in the radial direction) dominant only near the cold inner wall, as well as the curved arms of HTWs which were dominant in the whole area of the liquid pool. They confirmed this targetlike disturbance on the basis of linear stability analysis for the geometry of their experimental apparatus. Mukolobwiez, Chiffaudel and Daviaud (1998) observed HTWs traveling in the azimuthal direction in an annular pool of silicone oil (1.7mm in depth) heated from the inner wall.

Up to now, few experimental reports on thermal convection in low-Pr fluids such as liquid metals are known. Yamagishi and Fusegawa (1990) performed experiments with thermocapillary-buoyancy flow and observed dark lines at the surface of the melt by CCD camera during silicon Cz growth. Since this pattern looks like the spoke of a wheel, it is usually referred to as a "spoke" pattern. Nakamura, Eguchi, Azami and Hibiya (1999) reported thermal waves due to nonaxisymmetric flow at a Czochralski-type silicon-melt surface with a carbon-dummy crystal during the crucible rotation. It was found that the thermal wave number increased with increasing of the crucible rotation rate and the traveling rate of the thermal wave in the azimuthal direction was slower than the crucible rotation rate. Recently, Azami, Nakamura, Eguchi and Hibiya (2001) have observed spoke patterns on the surface of a shallow, annular pool of high-temperature silicon melt (3 and 8mm in depth) and reported that thermocapillary flow might play an important role in the incipience of three-dimensional convection and the number of spokes.

Numerical simulations have been also extensively used as a useful method to understand the details of thermocapillary or thermocapillary–buoyancy convection. Ben Hadid and Roux (1989, 1990, 1992) performed two-dimensional (2-D) simulations of thermocapillary–buoyancy and pure thermocapillary convection in pools of low-Pr fluids (Pr=0.015) with various aspect ratios, and showed the existence of multicellular steady flow and of a transition to oscillatory convection. Villers and Platten (1992) carried out both experiments and 2-D simulations for acetone (Pr=4), and confirmed the existence of multicellular flow. Peltier and Biringen (1993) reported their numerical results for 2-D oscillatory thermocapillary convection in rectangular cavities of different aspect ratios for the moderate-Pr-number fluid (Pr=6.78) and obtained a stability diagram (critical Marangoni number as a function of the aspect ratio).

Xu and Zebib (1998) performed 2-D and three-dimensional (3-D) calculations for fluids with $1<Pr<10$. They determined the Hopf bifurcation neutral curves as a function of the capillary Reynolds number and aspect ratio. Yi, Kakimoto, Eguchi, Watanabe, Shyo and Hibiya (1994) performed a 3-D numerical simulation of silicon melt flow and verified asymmetric temperature profiles similar to the spoke patterns and related asymmetric flow in the silicon melt. They concluded that the Rayleigh–Benard or Marangoni–Benard instability (or both) could cause spoke patterns in the silicon melt.

Tsukada, Kobayashi, Jing and Imaishi (2005) reported results of numerical simulation of CZ crystal growth of oxide. They discussed mechanism of spoke pattern and wave pattern within the framework of an unsteady three-dimensional analysis. It has been demonstrated numerically that the spoke pattern is due to Marangoni instability, while the wave pattern is cased by baroclinic instability.

Numerical results obtained by Bucchignani (2001) seem implausible because of their incredibly large temperature difference values (such as 372K over a wall distance of 30 mm) for the incipience of HTWs in a rectangular pool of silicone oil (Pr=13.9) under zero gravity, although they claimed that the wavelength and propagation angle were similar to those predicted by the LSA of Smith and Davis (1983), as well as the experimental results of Riley

and Neitzel (1998).

Sim, Zebib and Schwabe (2003), Li, Peng, Akiyama and Imaishi (2003) conducted numerical simulations of thermocapillary flow in an annular pool of silicone oil for the same geometry as that of Schwabe's experiment on FOTON-12, and compared their results with the FOTON-12 microgravity experiments. Shi and Imaishi (2006) reported 2-D and 3-D numerical simulations of thermocapillary flow, as well as buoyant thermocapillary flow, in a shallow annular pool of silicone oil (Pr=6.7, depth of 1.0 mm) heated at the outer wall and cooled at the inner wall. With this small depth, they believed that the thermocapillary force was dominant and the buoyant force could be negligible because of its small dynamic Bond number (Bo_d=0.125). Li, Peng, Wu, Imaishi and Zeng (2004), Li, Imaishi, Azami and Hibiya (2004) also conducted a series of numerical simulations for annular pools of low-Pr silicon melts (Pr=0.011) heated from the outer wall.

In the present paper, we survey our recent numerical studies of thermal convection in annular pools. The mechanism of convective instability in annular pools is discussed and the critical conditions for the onset of three-dimensional flow are determined.

2 Model formulation

2.1 Basic assumptions and governing equations

We analyze the flow in an annular pool of depth d, inner radius r_i and outer radius r_o, with a free upper surface and solid bottom wall, as shown schematically in Fig. 1. The inner and outer cylinders are maintained at constant temperatures T_c and T_h, $(T_h > T_c)$, respectively. The horizontal temperature gradient varies in the radial direction. Convection is generated by both the surface tension gradient on the top surface and thermal buoyancy. The following assumptions are introduced in our model:

1) The fluid is an incompressible Newtonian fluid and a constant property assumption is applicable with the exception of the surface tension and the buoyancy term. 2) The velocity is small and the flow is laminar. 3) The upper surface is flat and nondeformable. 4) At the free surface, the thermocapillary force is taken into account. At other solid-liquid boundaries, a no-slip condition is applied. 5) Both bottom and top boundaries are assumed to be adiabatic.

With the above assumptions, the flow and heat transfer equations are expressed in a nondimensional form as follows:

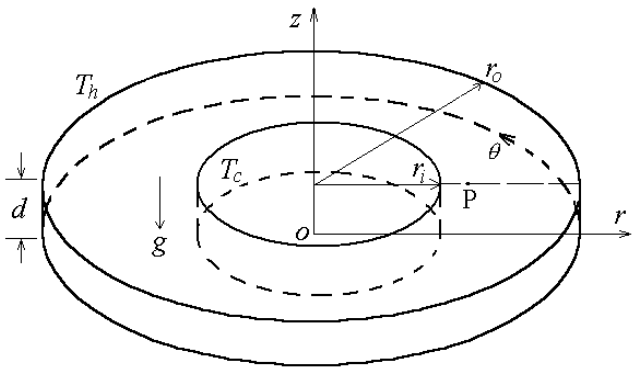

Figure 1 : Configuration of model system

$$\nabla \cdot \mathrm{V} = 0, \tag{1}$$

$$\frac{\partial \mathrm{V}}{\partial \tau} + \mathrm{V} \cdot \nabla \mathrm{V} = -\nabla P + \nabla^2 \mathrm{V} + Gr\Theta \mathrm{e}_Z, \tag{2}$$

$$\frac{\partial \Theta}{\partial \tau} + \mathrm{V} \cdot \nabla \Theta = \frac{1}{\mathrm{Pr}} \nabla^2 \Theta. \tag{3}$$

The boundary conditions at the free surface ($Z = d/r_o$, $R_i < R < 1$, $0 \le \theta < 2\pi$)

$$\frac{\partial V_R}{\partial Z} = -\frac{Ma}{\mathrm{Pr}} \frac{\partial \Theta}{\partial R}, \tag{4a}$$

$$\frac{\partial V_\theta}{\partial Z} = -\frac{Ma}{\mathrm{Pr}} \frac{\partial \Theta}{R \partial \theta}, \tag{4b}$$

$$V_Z = 0, \tag{4c}$$

$$\frac{\partial \Theta}{\partial Z} = 0, \tag{4d}$$

at the bottom ($Z = 0$, $R_i < R < 1$, $0 \le \theta < 2\pi$)

$$V_R = 0, \tag{5a}$$

$$V_\theta = 0, \tag{5b}$$

$$V_Z = 0, \tag{5c}$$

$$\frac{\partial \Theta}{\partial Z} = 0, \tag{5d}$$

at the inner cylinder ($R = R_i$, $0 \le Z \le d/r_o$, $0 \le \theta < 2\pi$)

$$V_R = 0, \tag{6a}$$

$$V_\theta = 0, \tag{6b}$$

$$V_Z = 0, \tag{6c}$$

$$\Theta = \Theta_i = 0, \tag{6d}$$

and at the outer cylinder ($R = 1$, $0 \le Z \le d/r_o$, $0 \le \theta < 2\pi$)

$$V_R = 0, \tag{7a}$$

$$V_\theta = 0, \tag{7b}$$

$$V_Z = 0, \tag{7c}$$

$$\Theta = \Theta_o = 1. \tag{7d}$$

The initial conditions are expressed as follows (at τ=0):

$$V_R = 0, \tag{8a}$$

$$V_\theta = 0, \tag{8b}$$

$$V_Z = 0, \tag{8c}$$

$$\Theta = 1 - \ln R / \ln R_i. \tag{8d}$$

Where $\boldsymbol{V}$ is the velocity vector, P the pressure, Θ the temperature, τ the time in nondimensional form. R, Z and θ are the cylindrical coordinates. $\boldsymbol{e}_Z$ is the Z-directional unit vector.

The variables are nondimensionalized as

$$(R,Z) = \frac{(r,z)}{r_o}, \quad (V_R, V_\theta, V_Z) = \frac{(v_r, v_\theta, v_z)}{\nu / r_o},$$

$$P = \frac{p r_o^2}{\rho \nu^2}, \quad \Theta = \frac{T - T_c}{T_h - T_c}, \quad \tau = \frac{t\nu}{r_o^2}.$$

The dimensionless parameters are defined as follows:

Grashof number:

$$Gr = \frac{\rho_T g \Delta T r_o^3}{\nu^2}, \tag{9}$$

Marangoni number:

$$Ma = \frac{\gamma_T \Delta T r_o}{\mu \alpha}, \tag{10}$$

Prandtl number:

$$\mathrm{Pr} = \frac{\nu}{\alpha}, \tag{11}$$

Dynamic Bond number:

$$Bo_d = \frac{\rho g \rho_T d^2}{\gamma_T}. \tag{12}$$

Where $\Delta T = T_h - T_c$. ρ is the density, ν the kinematic viscosity, ρ_T the thermal expansion coefficient, μ the dynamic viscosity, α the thermal diffusivity, γ_T the surface tension coefficient.

2.2 Numerical method

The fundamental equations are discretized by a finite-volume method. The modified central difference approximation is applied to the diffusion terms while the QUICK scheme is used for the convective terms. The HSMAC algorithm is used to correct simultaneously the pressure and the velocities. To solve Poisson equation, the preconditioned Bi-CGSTAB algorithm is applied. In this study, nonuniform staggered grids of $62^r \times (22\text{-}42)^z \times 63^\theta$ for the silicon melt and $102^r \times (16\text{-}36)^z \times 243^\theta$ for silicone oil were used with finer meshes in the regions under the free surface and near the bottom and sidewalls. The validation of the code and convergence of grids for the thermal convection simulation were checked. The numerical simulations were conducted on a Fujitsu VPP5000/64 supercomputer at the Computing and Communications Center of Kyushu University.

Table 1 : Geometric parameters and physical properties for the silicon melt case

Geometry parameters
Inner radius, r_i=15 mm, outer radius, r_o=50 mm
Depth, d=3, 8 mm
Physical properties
Prandtl number Pr=0.011
Viscosity, μ =7.0$\times 10^{-4}$ kg m^{-1}s^{-1}
Density, ρ=2530 kg m^{-3}
Thermal expansion coefficient, ρ_T=1.5$\times 10^{-4}$ K^{-1}
Surface tension coefficient, γ_T=-7.0$\times 10^{-5}$ N m^{-1} K^{-1}

Table 2 : Geometric parameters and physical properties for the silicone oil case

Geometry parameters
Inner radius, r_i=20 mm, outer radius, r_o=40 mm
Depth, d=1-11 mm
Physical properties
Prandtl number Pr=6.7
Kinematic viscosity, ν=6.5$\times 10^{-7}$ m^{2}s^{-1}
Density, ρ=760 kg m^{-3}
Thermal expansion coefficient, ρ_T=1.34$\times 10^{-3}$ K^{-1}
Surface tension coefficient, γ_T=-8.0$\times 10^{-5}$ N m^{-1} K^{-1}

The geometric parameters used in this work and the ther-

mophysical properties of silicon melt at 1683 K and silicone oil at 20^{o}C are listed in Table 1 and 2, respectively.

3 Results and discussion

3.1 Basic flow

When the radial temperature gradient (ΔT) is small, the flow is steady and axisymmetric. This type of flow is referred to as the "basic flow". In the present configuration, the basic flow appears as an axisymmetric steady radial flow with a single convection roll cell. The surface fluid flows from the outer cylinder wall toward the inner cylinder wall and a return flow is established near the bottom. The strength of the basic flow increases as ΔT increases. A second co-rotating roll cell embedded in the large-scale flow appears when ΔT is increased (see the "eye" in Fig. 2). The maximum stream function of the basic flow (the eye) occurs near the inner cylinder and the outer cylinder for the silicon melt and silicone oil, respectively.

For the silicon melt, the temperature distribution in the radial direction is almost independent of the presence of the melt flow and tends to that of conductive heat transfer, as shown in Fig. 3(a), because the thermal conductivity of the silicon melt is large. In this case, isotherms are almost composed of vertical lines.

For silicone oil, thermal boundary layers appear near the inner and outer cylinders, because of the low thermal conductivity. Large temperature drops occur in those boundary layers so that the effective temperature gradient in the middle part of the annular surface is smaller than the superficial temperature gradient $(\Delta T/(r_o - r_i))$ based on the imposed temperature difference ΔT. When the liquid depth is more than 6 mm, the surface temperature gradient in the middle part of the annular pool is practically zero and the temperature drops are concentrated in the vertical thermal boundary layers near the inner and outer walls. Because large radial temperature drops appear near the inner and outer cylinders, the surface velocity exhibits a sharp peak near the inner cold wall, as shown in Fig. 3(b).

Figure 4 shows the radial velocity component as a function of z/d at the middle of annular pools. In both cases, the thermal convection generates an inward radial flow for about $z/d > 2/3$ and a return flow for about $z/d < 2/3$.

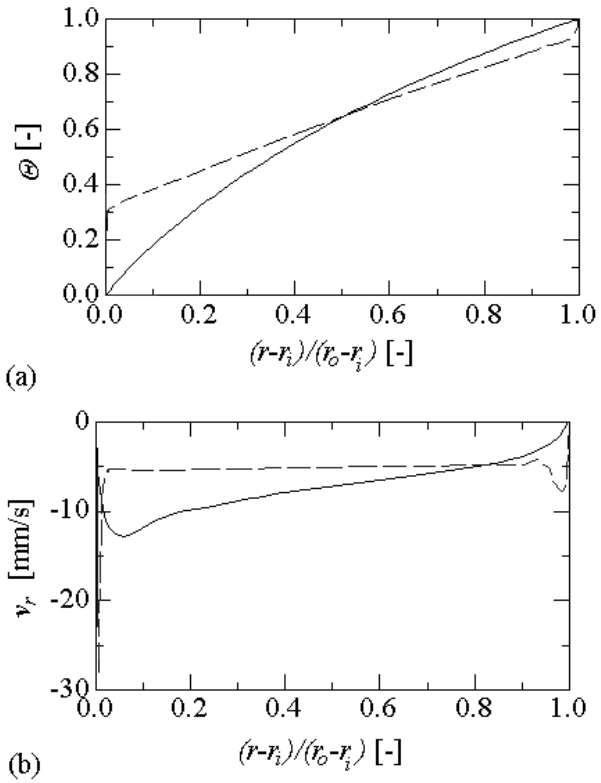

Figure 3 : Temperature (a) and radial velocity component (b) as a function of $(r - r_i)/(r_o - r_i)$ on the free surface. Solid line: silicon melt, d=3mm, ΔT=4K. Dot line: silicone oil, d=1mm, ΔT=4K.

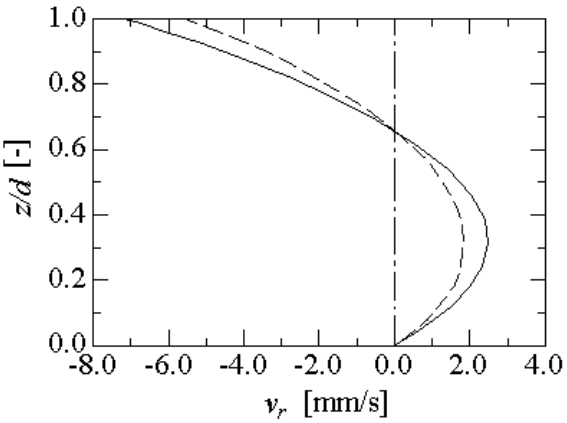

Figure 4 : Radial velocity component as a function of z/d at the middle of the annular pools. Solid line: silicon melt, d=3mm, ΔT=4K. Dot line: silicone oil, d=1mm, ΔT=4K.

3.2 Critical condition for flow transition

When the temperature difference exceeds a certain threshold value, 3-D disturbances are incubated and their

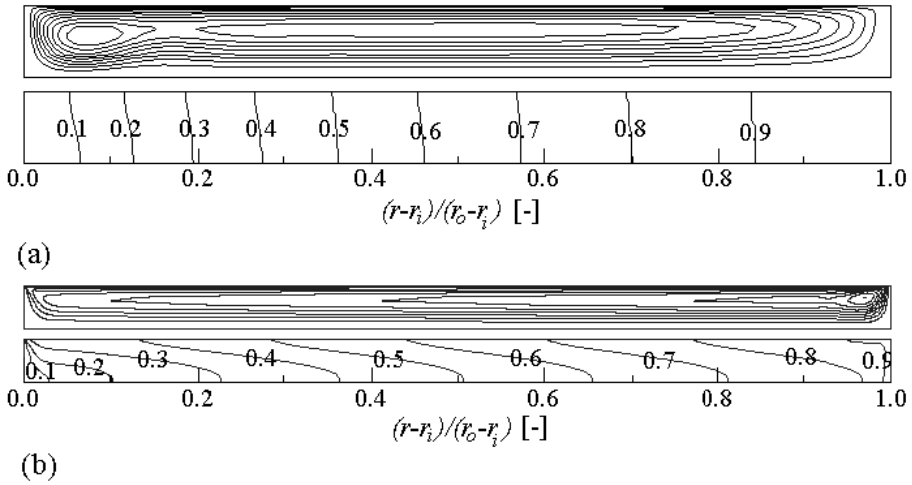

Figure 2 : Streamlines and isotherms of the basic flow. (a) Silicon melt, d=3mm, ΔT=4K, ψ_{max}=121mm^3/s; (b) Silicone oil, d=1mm, ΔT=4K, ψ_{max}=328mm^3/s (ψ is the stream function).

amplitudes increase with time. Finally, the flow undergoes transition to various 3-D patterns. Present numerical simulations with the large temperature difference show that during the initial growth processes the intensity X of any disturbance can be expressed by Eq. (13) and (14) for three-dimensional oscillatory flow (3DOF) and three-dimensional steady flow (3DSF), respectively,

$$X(r,\theta,z,t) = X_0(r,\theta,z)\exp[(\beta + i\beta_I)t)], \quad (13)$$

$$X(R,\theta,Z,\tau) = X_0(R,\theta,Z,0)\sin(2\pi m\theta)\exp(\beta\tau). \quad (14)$$

where β is the growth rate constant of the disturbance, β_I represents the time dependent oscillatory characteristics of the disturbance and m is the wave number.

For each value of ΔT, we can determine the growth rate constant β as the slope of a plot of the logarithm of a local value of surface velocity as a function of time. A plot of β vs. ΔT reveals the critical temperature difference for the incipience of 3-D flow, (ΔT_{cri}), as the ΔT at which β becomes zero (since the state β=0 corresponds to a marginal stability limit). For the silicon melt pool of d=3mm, the critical temperature is 5.32K. For the silicone oil pool of d=1-11mm, the simulation results of the critical temperature difference are shown in Fig. 5. It can be seen that the critical values obtained in the present simulation show a good agreement with the experimental ones obtained by Schwabe (2002) at d>5mm. For shallow pools, the simulation results are slightly larger than the experiments. For the pool of d=1mm, ΔT_{cri} obtained by Shi and Imaishi (2006) with grids of $202^r \times 16^z \times 603^\theta$ is also shown in Fig. 5.

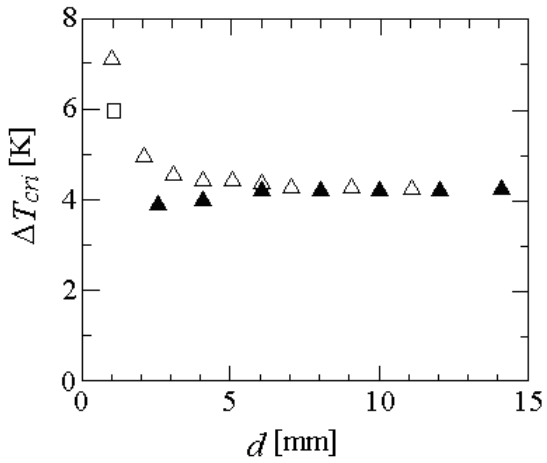

Figure 5 : Comparison of simulation results and experimental results (critical temperature difference for silicone oil). : Experimental results [Schwabe (2002)]; : Simulation results; : Simulation results [Shi and Imaishi (2006)].

3.3 Three-dimensional flow

3.3.1 Results of silicon melt

Figure 6 shows the simulation results for d=3 mm, including the snapshots of the surface temperature fluctuation δT (left side) and a space-time diagram (STD) of the surface temperature along a circumference at r=20 mm (right side). The surface temperature fluctuation δT is

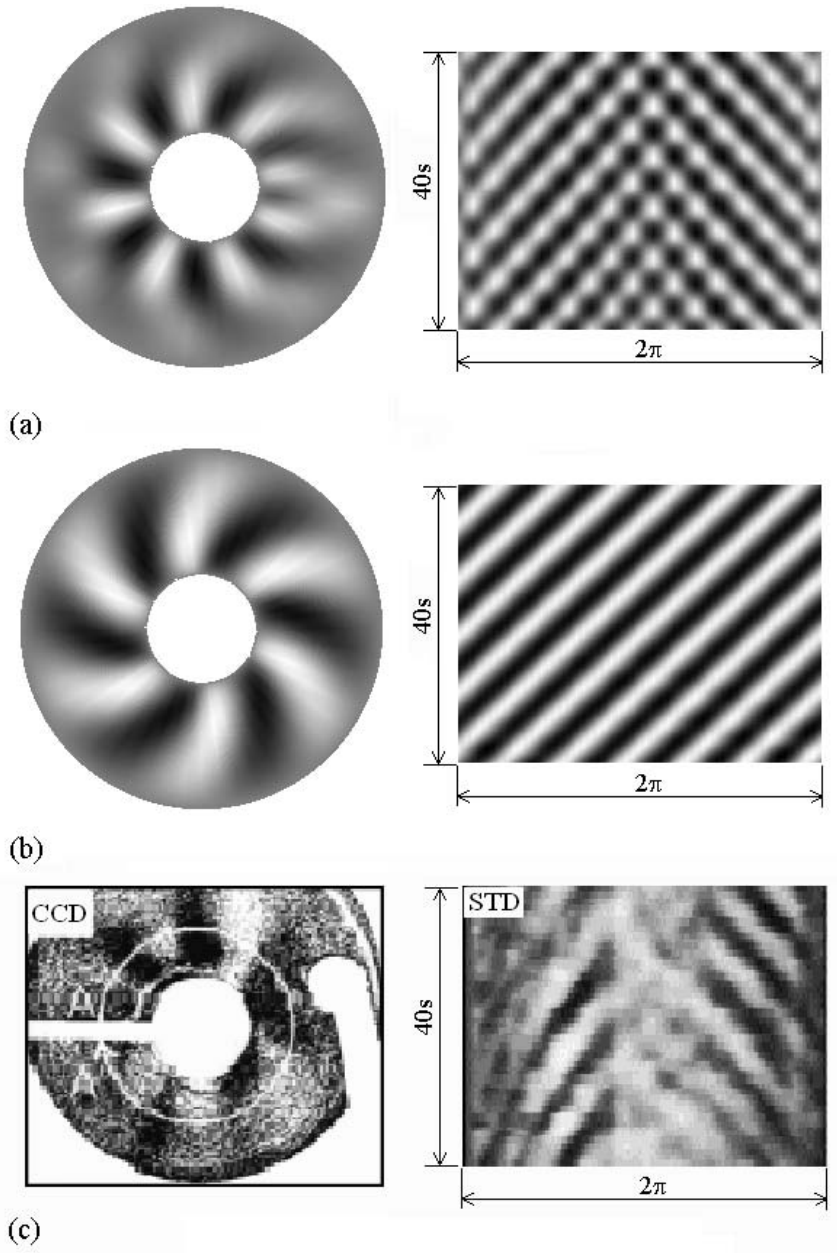

Figure 6 : Snapshots of surface temperature fluctuation and space-time diagram of surface temperature distribution for the layer of d=3 mm at r=20 mm. (a) ΔT=12K. (b) ΔT=21K. (c) Experimental result of Azami, Nakamura, Eguchi and Hibiya (2001).

introduced in order to extract the 3-D disturbances:

$$\delta T(r,\theta,d,t) = T(r,\theta,d,t) - \frac{1}{2\pi}\int_0^{2\pi} T(r,\theta,d,t)d\theta. \qquad (15)$$

When the temperature difference exceeds the critical value, many traveling curved spoke patterns are observed on the entire surface. These correspond to the "hydrothermal wave" instability. When the radial temperature difference is small but above the critical condition, for example, ΔT=12 K, as shown in Fig. 6(a), the traveling waves originate from around θ=0 and travel toward θ=π via two paths. One wave group is propagating in the clockwise direction and the other in the counterclockwise one. The angles (ϕ) between wave propagation and the radial direction, measured at$r$=20 mm,

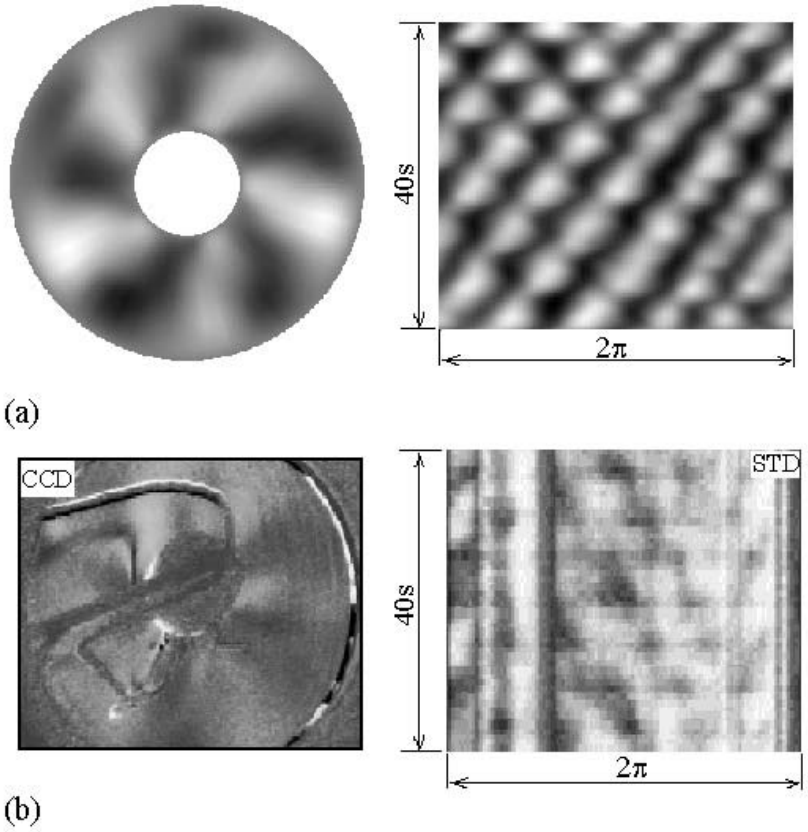

Figure 7 : Snapshots of surface temperature fluctuation and space-time diagram of surface temperature distribution for the layer of d=8 mm at$r$=20 mm. (a) ΔT=21K. (b) Experimental result of Azami, Nakamura, Eguchi and Hibiya (2001).

are about 75^o-80^o and 100^o-105^o, respectively. Under a much larger radial temperature gradient, as shown in Fig. 6(b) for ΔT=21 K, the hydrothermal waves propagate along the counter-clockwise direction and the angle ϕ is approximately 78^o at r=20 mm, which is close to the angle of 80^o predicted by the linear stability theory for the infinite rectangular layer. However, as seen from Figs. 6(a) and 6(b), the spokes are not straight but bent. Because the temperature at the free surface is always higher than that at the bottom surface, therefore, the instability is induced by the hydrothermal wave instability. These traveling waves appear as many parallel tilted straight lines on the STD taken at r=20 mm. The present result at ΔT=12 K in Fig. 6(a) is very close to the experimental result of Azami, Nakamura, Eguchi and Hibiya (2001) (shown in Fig. 6(c)) in an annular pool with r_i=15mm and r_o=63.5 mm. The surface patterns look similar. However the number of spoke patterns and the traveling speeds in the azimuthal direction (i.e. slope of the STD lines) in the present simulation are higher than those of experiments. Differences in the size, uncertainties in the thermal boundary conditions in the experiments and also the uncertainty related to the temperature coefficient of surface tension of silicon melt may be thought of as the causes at the basis of the discrepancy.

In layers of d=8 mm (seethe snapshots in Fig. 7(a)), the spoke patterns become straight and broad. These spoke patterns also move in the azimuthal direction. But, they exhibit combined a standing wave type oscillation, i.e., periodic growth and decay of temperature disturbances, with the azimuthal propagation. Then, the STD is composed of inclined lines slightly fluctuating in amplitude and direction. Obviously, it is not the "hydrothermal wave" instability. Perhaps, in this case the buoyancy force interacts with the Marangoni effect to generate a quasi stable traveling 3-D disturbance moving in the azimuthal direction like the hydrothermal wave.

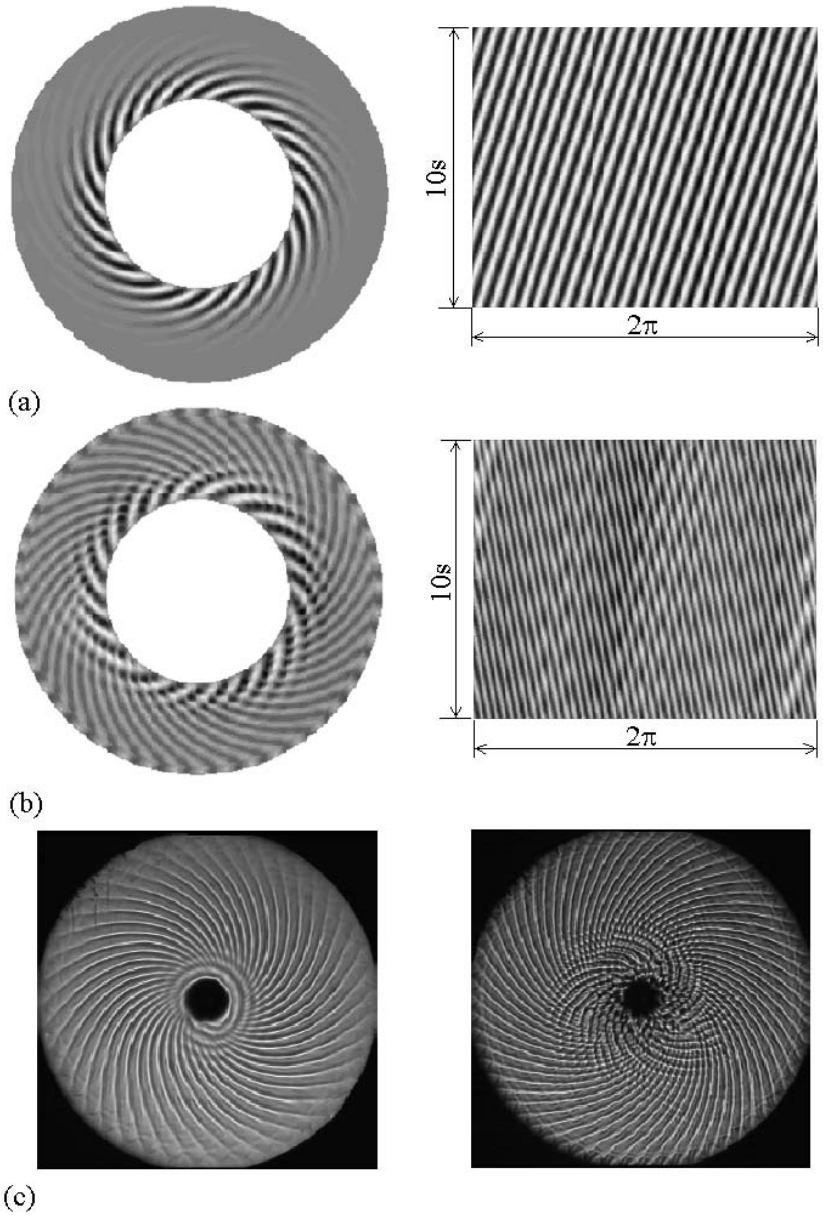

Figure 8 : Snapshots of surface temperature fluctuation and space-time diagram of surface temperature distribution at r=25mm. (a) d=1mm, ΔT=8K; (b) d=1mm, ΔT=12K; (c) Experimental results [Garnier and Chiffaudel (2001)], left: d=1.9mm, ΔT=14.25K, right: d=1.2mm, ΔT=20K.

3.3.2 Results of silicone oil

Figure 8 shows the characteristics of 3-D oscillatory flow in a very thin annular pool of d=1mm, including the snapshots of the surface temperature fluctuation distribution and the space-time diagram (STD) of the surface temperature distribution along a circumference at r=25mm. In this case, the Bo_d number is about 0.125, and the thermocapillary force is dominant. Therefore, traveling curved spoke patterns on the free surface also correspond to the "hydrothermal wave" instability.

Under a small temperature difference (ΔT) number, for example, ΔT=8K, the hydrothermal waves propagate in the counterclockwise direction, as shown in Fig. 8(a). In this case, the HTW patterns are clearly observable only in the inner part of the pool, being faded in the outer region. The angle (ϕ) between the wave propagation and the ra-

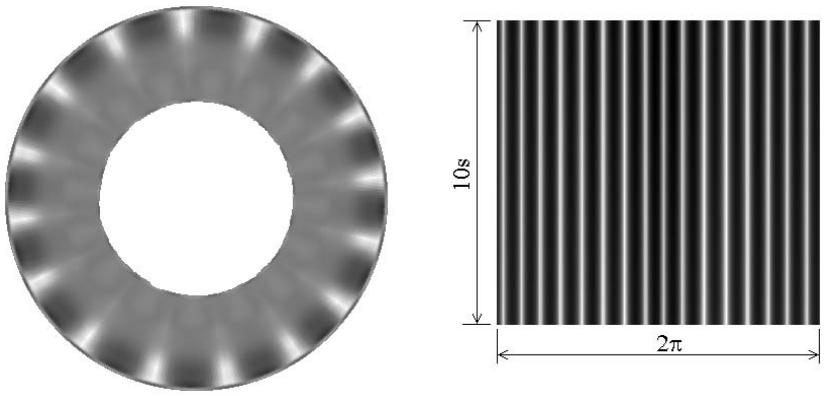

Figure 9 : Snapshots of surface temperature fluctuation and space–time diagram of surface temperature distribution at r=25mm for the 3DSF. d=6mm, ΔT=10K.

dial direction, measured at r=25mm, is about 155^o-160^o, which is close to those predicted by the linear stability theory for the infinite rectangular layer for Pr=10 [Smith and Davis (1983)] and the experimental result (0.83π) obtained in a rectangular pool of silicone oil (Pr=10.3) [Burguete, Mukolobwiez, Daviaud, Garnier, and Chiffaudel (2001)]. As ΔTincreases, HTWs become dominant over the whole area of the liquid surface and the azimuthal wave number will decrease.

The simulation with a larger ΔT, such as ΔT=12K, indicates two groups of HTWs coexisting in the pool with different wave numbers and different traveling directions, as shown in Fig. 8(b). Interferences between two groups of HTWs occur throughout almost the entire volume of the pool. The coexistence of two groups of HTWs was also reported by Garnier and Chiffaudel (2001), as shown in Fig. 8(c), although their pool geometry is different from that of the present system. However, we do not observe the "target-like (coaxial) waves" propagating outward in the radial direction, which were reported by Garnier and Chiffaudel (2001) near the inner wall of their annular pool which had much larger outer wall and smaller inner wall radiuses. The larger inner wall radius in the present system can produce a surface temperature gradient near the inner wall that is less than the critical value, which is necessary for the incipience of the targetlike waves.

For the deep layers with $d \geq$5mm, the simulation results are different from those with d=1mm and from those discussed before for silicon melt with d=8mm. Fig. 9 shows the snapshot of the surface temperature fluctuation distribution and the STD of the surface temperature along a circumference at r=25mm for the layer of d=6mm at ΔT=10K. In this case, many straight spoke patterns are observed over the entire surface area, but they do not move. As a result, the STD appears as many vertical lines. The number of the spoke patterns is about 16 and independent on the temperature difference and the pool depth. This flow pattern belongs to a three-dimensional steady flow. The mechanism is explained as follows.

The Marangoni effect generates an inward radial flow (Hereafter we denote this as the Ma-driven flow) near the free surface. Therefore, the temperature at the free surface is always higher than that at the bottom. Because the radial temperature drops are mainly concentrated in the vertical thermal boundary layers near the inner and outer walls, the flow driven by the buoyancy force (the B-driven flow) near the hotter wall carries low temperature liquid to the area below the free surface, as shown in Fig. 10(a). At the same time, there is a return flow carrying high temperature liquid to the area below the B-driven flow. Therefore, there exists a region with a counter temperature gradient near the hot wall (its depth is assumed to be d_c, as shown in Fig. 10(b)). In the counter temperature gradient layer, Rayleigh-Benard instability can be produced when the Rayleigh (Ra) number exceeds a certain threshold value. Figure 10(c) suggests that the 3DSF consists of pairs of counter-rotating longitudinal rolls (whose axes are oriented parallel to the applied temperature gradient) that are superimposed on the basic flow, and this result has a good agreement with the experiment of Benz and Schwabe (2001). In order to prove that the 3DSF corresponds to the Rayleigh-Benard instability, the local Ra number is estimated.

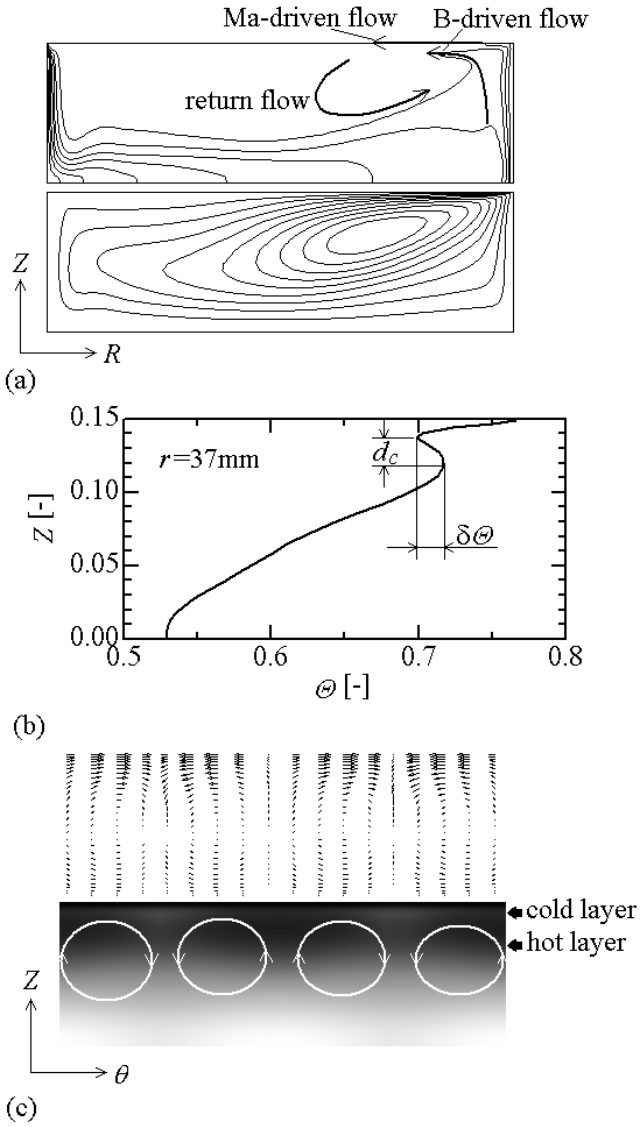

Figure 10 : The mechanism of the 3DSF. d=6mm, ΔT=10K. (a) Isotherms and pseudo-streamlines at the plane of θ=0. (b) Temperature as a function of Z at θ=0. (c) Counter-rotating longitudinal rolls at r=37mm at the plane of Z-θ.

When d=6mm and ΔT=6K, the maximum depth d_c of the counter temperature gradient layer is found to be about 2.32 mm and the maximum vertical temperature difference δT_c is estimated to be 0.28K from the simulated results. In this case, the local Rayleigh number defined as Ra=$g\rho_T \delta T d_c^3/(\nu\alpha)$, is about 728. It implies that the local Ra number will exceed the critical Ra number value, Ra_{cri}=657.5, which is obtained by the linear stability analysis [Zeng (1999)] for the incipience of the Rayleigh-Benard instability in an infinitely extended fluid layer with the free upper and nether surfaces subject to a constant vertical temperature gradient. This indicates that the 3DSF is the result of the Rayleigh-Benard instability within the counter temperature gradient layer.

When $2 \leq d \leq 4$, combined hydrothermal waves and 3-D oscillatory flow appear on the free surface, as shown in Fig. 11(a). The present results are similar with results of 2-D non linear numerical simulations for a rectangular liquid layer with Pr=14 and aspect ratio A=25 performed by Shevtsova, Nepomnyashchy and Legros (2003). In this case, the vertical temperature gradient near the inner wall is large enough to form the "hydrothermal wave" instability. Therefore, HTW patterns are clearly observable in the inner part of the pool. But, the counter temperature gradient layer near the hotter wall also exists, as shown in Fig. 11(b). Accordingly, pairs of counter-rotating longitudinal rolls are dominant in this region. These rolls will propagate in the azimuthal direction driven by HTWs (and owing to such a rotation the axes of rolls are not parallel to the temperature gradient). In this case, the wave number of the 3DOF is the same as that of HTWs.

4 Conclusions

A series of 3-D numerical simulations of the thermal convections in annular pools have been conducted by means of a finite volume method. From the simulation results, the following conclusions have been obtained.

1. For the low-Pr silicon melt, in a shallow annular pool of d=3 mm, hydrothermal waves appear and travel in the azimuthal direction when the temperature difference exceeds the critical value. In a thick pool of d=8 mm, there appears a standing wave type of oscillatory longitudinal rolls, which moves in the azimuthal direction and looks very similar to the hydrothermal waves.

2. For the moderate-Pr silicone oil, in a shallow pool (d=1mm), a hydrothermal wave characterized by curved spokes is dominant. Under small ΔTnumber, there is only one group of HTWs. The azimuthal wave number decreases and oscillation frequency increases as ΔTincreases. Under larger ΔT, two groups of HTWs with different wave numbers and different traveling directions coexist in the pool. When $2 \leq d \leq 4$mm, the HTW and a 3DOF (3D oscillatory flow) with radial rolls coexist in the pool

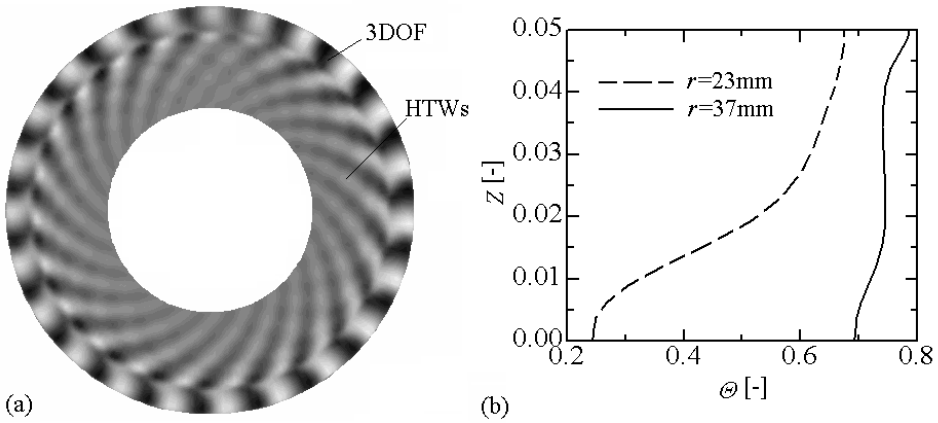

Figure 11 : Combined hydrothermal waves and 3-D oscillatory flow at d=2mm and ΔT=10K. (a) Snapshots of surface temperature fluctuation. (b) Temperature as a function of Z at θ=0.

and travel in the same azimuthal direction with the same angular velocity. In this case, the wave number of the 3DOF is the same as that of the HTW. In deep pools ($d \geq$5mm) a 3DSF (3D steady flow) appears. This flow pattern corresponds to the Rayleigh-Benard instability, which consists of pairs of counter-rotating longitudinal rolls. The number of the spoke patterns is independent on $\Delta T$and the pool depth d.

Acknowledgement: This work is supported by National Natural Science Foundation of China (grant number 50476042) and the Scientific Research Foundation for the Returned Overseas Chinese Scholars, State Education Ministry.

References

Azami, T.; Nakamura, S.; Eguchi, M.; Hibiya, T. (2001): The role of surface-tension-driven flow in the formation of a surface pattern on a Czochralski silicon melt. *J. Crystal Growth*, vol. 233, pp. 99-107.

Ben Hadid, H.; Roux, B., (1989): Buoyancy- and thermocapillary-driven flows in a shallow open cavity: Unsteady flow regimes. *J. Crystal Growth*, vol. 97, pp. 217-225.

Ben Hadid, H.; Roux, B., (1990): Thermocapillary convection in long horizontal layers of low-Prandtl number melts subject to a horizontal temperature gradient. *J. Fluid Mech.*, Vol. 221, pp. 77-103.

Ben Hadid, H.; Roux, B., (1992): Buoyancy- and thermocapillary-driven flows in differentially heated cavities for low-Prandtl-number fluids. *J. Fluid Mech.*, vol. 235, pp. 1-36.

Benz, S.; Hintz, P.; Riley, R. J.; Neitzel G. P. (1998): Instability of thermocapillary-buoyancy convection in shallow layers. Part 2. Suppression of hydrothermal waves. *J. Fluid Mech.*, vol. 359, pp. 165-180.

Benz, S.; Schwabe, D. (2001): The three-dimensional stationary instability in dynamic thermocapillary shallow cavities. *Experiments in Fluids*, vol. 31, pp. 409-416.

Burguete, J. (2001): Numerical characterization of hydrothermal waves in a laterally heated shallow layer. *Phys. Fluids*, vol. 13, pp. 3839-3849.

Burguete, J.; Mukolobwiez, N.; Daviaud, F., Garnier, N.; Chiffaudel, A. (2001): Buoyant-thermocapillary instabilities in extended liquid layers subjected to a horizontal temperature gradient. *Phys. Fluids*, vol. 13, pp. 2773-2787.

Garnier, N.; Chiffaudel, A. (2001): Two dimensional hydrothermal waves in an extended cylindrical vessel. *Eur. Phys. J. B*, vol. 19, pp. 87-95.

Garnier, N.; Normand, C. (2001): Effects of curvature on hydrothermal waves instability of radial thermocapillary flows. *C. R. Acad. Sci. Paris*, vol. 2, pp. 1227-1233.

Hoyas, S., Herrero, H., Mancho, A. M. (2002a): Bifurcation diversity of dynamic thermocapillary liquid layers. *Phys. Rev. E.*, vol. 66, 057301-1-4.

Hoyas, S., Herrero, H., Mancho, A. M. (2002b): Thermal convection in a cylindrical annulus heated laterally. *J. Phys. A*, vol. 35, pp. 4067-4083.

Kamotani, Y. (1999): Thermocapillary flow under microgravity - experimental results. *Adv. Space Res*., vol. 24, pp. 1357-1366.

Laure, P.; Roux, B. (1989): Linear and non-linear analysis of the Hadley circulation, *J. Crystal Growth*, vol. 97, pp. 226-234.

Li, Y. R.; Imaishi, N.; Azami, T.; Hibiya, T. (2004): Three-dimensional oscillatory flow in a thin annular pool of silicon melt. *J. Crystal Growth*, vol. 260, pp. 28-42.

Li, Y. R.; Peng, L.; Akiyama, Y.; Imaishi, N. (2003): Three-dimensional numerical simulation of thermocapillary flow of moderate Prandtl number fluid in an annular pool. *J. Crystal Growth*, vol. 259, pp. 374-387.

Li, Y. R.; Peng, L.; Wu, S. Y.; Imaishi, N.; Zeng, D. L. (2004): Thermocapillary-buoyancy flow of silicon melt in a shallow annular pool. *Cryst. Res. Technol.*, vol. 39, pp. 1055-1062.

Mukolobwiez, N.; Chiffaudel, A.; Daviaud, F. (1998): Supercritical Eckhaus Instability for Surface-Tension-Driven Hydrothermal Waves. *Phys. Rev. Letters*, vol. 80, pp. 4661-4664.

Nakamura, S.; Eguchi, M.; Azami, T.; Hibiya, T. (1999): Thermal waves of a nonaxisymmetric flow in a Czochralski-type silicon melt. *J. Crystal Growth*, vol. 207, pp. 55-61.

Parmentier, P. M.; Reynier, V. C.; Lebon, G. (1993): Buoyant-thermocapillary instabilities in medium Prandtl number fluid layers subject to a horizontal temperature gradient. *Int. J. Heat Mass Transfer*, vol. 36, pp. 2417-2427.

Peltier, L. J.; Biringen, S. (1993): Time-dependent thermocapillary convection in a rectangular cavity: numerical results for a moderate Prandtl number fluid. *J. Fluid Mech.*, vol. 257, pp. 339-357.

Riley, R. J.; Neitzel, G. P. (1998): Instability of thermocapillary-buoyancy convection in shallow layers. Part 1. Characterization of steady and oscillatory instabilities. *J. Fluid Mech.*, vol. 359, pp. 143-164.

Smith, M. K.; Davis, S. H. (1983): Instabilities of dynamic thermocapillary liquid layers. Part 1: convective instabilities. *J. Fluid Mech.*, vol. 132, pp. 119-144.

Schwabe, D. (2002): Buoyant-thermocapillary and pure thermocapillary convective instabilities in Czochralski systems. *J. Crystal Growth*, vol. 237, pp. 1849-1853.

Schwabe, D.; Benz, S. (2002): Thermocapillary flow instabilities in an annulus under microgravity - Results of the experiment magia. *Adv. Space Res.*, vol. 29, pp. 629-638.

Schwabe D.; Moller U.; Schneider J.; Scharmann A. (1992): Instabilities of shallow dynamic thermocapillary liquid layers. *Phys. Fluids A*, vol. 4, pp. 2368-2381.

Schwabe D.; Zebib A.; Sim B. C. (2003): Oscillatory thermocapillary convection in open cylindrical annuli. Part 1. Experiments under microgravity. *J. Fluid Mech.*, vol. 491, pp. 239-258.

Shevtsova, V.M.; Nepomnyashchy, A.A.; Legros, J.C. (2003): Thermocapillary-buoyancy convection in a shallow cavity heated from the side. *Phys. Rev. E*, vol. 67: 066308.

Shi, W. Y.; Imaishi, N. (2006): Hydrothermal waves in differentially heated shallow annular pools of silicone oil. *J. Crystal Growth*, vol. 290, pp. 280-291.

Sim, B. C.; Zebib, A.; Schwabe, D. (2003): Oscillatory thermocapillary convection in open cylindrical annuli. Part 2. Simulations. *J. Fluid Mech.*, vol. 491, pp. 259-274.

Tsukada, T.; Kobayashi, M.; Jing; C.J.; Imaishi, N. (2005): Numerical simulation of CZ crystal growth of oxide. *FDMP: Fluid Dyn. Mater. Process*, vol. 1, pp.45-62.

Villers, D.; Platten, J. (1992): Coupled Buoyancy and Marangoni convection in acetone: experiments and comparison with numerical simulations, *J. Fluid Mech.*, Vol. 234, pp. 487-510.

Xu, J.; Zebib, A. (1998): Oscillatory two- and three dimensional thermocapillary convection. *J. Fluid Mech.*, vol. 364, pp. 187-209.

Yamagishi, H.; Fusegawa, I. (1990): Experimental observation of a surface pattern on Czochralski silicon melt. *J. Jpn. Assoc. Crystal Growth*, vol. 17, pp. 304-311.

Yi, K. W.; Kakimoto, K.; Eguchi, M.; Watanabe, M.; Shyo, T.; Hibiya, T. (1994): Spoke patterns on molten silicon in Czochralski system. *J. Crystal Growth*, vol. 144, pp. 20-28.

Zeng, D. L. (1999): Engineering Nonequilibrium Thermodynamics, Science China Press, Beijing, pp. 187-201.